Journal of Circuits, Systems, and Computers
Vol. 31, No. 5 (2022) 2250085 (32 pages)
© World Scientific Publishing Company
DOI: 10.1142/S0218126622500852

Multi-Scroll Attractors with Hyperchaotic Behavior Using Fractional-Order Systems*

Kenan Altun

Department of Electronics and Automation,
Vocational School of Technical Sciences,
Sivas Cumhuriyet University, 58140, Turkey
kaltun@cumhuriyet.edu.tr

Received 7 June 2021
Accepted 14 September 2021
Published 28 October 2021

In this paper, a systematic design is proposed to generate multi-scroll attractors with hyperchaotic behavior using fractional-order systems, in which switched SC-CNN is triggered with error function. Sprott Systems Case H is reconstructed with fractional-order switched SC-CNN system. Herein, the goal is to increase the complexity of chaotic signals, hence providing safer and reliable communication by generating multi-scroll attractors with hyperchaotic behavior using fractional-order systems. Theoretical analysis of the proposed system's dynamical behaviors is scrutinized, while numerical investigations are carried out with equilibrium points, Lyapunov exponent, bifurcation diagrams, Poincaré mapping and 0/1 test methods. Numerical results are validated through simulations and on an FPAA platform.

Keywords: Error function; FPAA; fractional-order; hyperchaos; multi-scroll chaotic attractors; CNN.

1. Introduction

An information signal is transmitted with a carrier signal in a communication system. The carrier signal's predictability level describes the level of communication safety and reliability.[1] In a chaotic-based communication system, chaotic signal accounts for the carrier signal to transmit the information signal.[2] Herein, lowering the predictability level of chaotic signal amounts to safer communication.[1,3–5] Actually, lowering the predictability level of chaotic signal means increasing the complexity of the chaotic signal. In recent years, the security defects of chaotic cryptosystem and chaotic communication built using single or double-dimensional chaotic systems emerged due to their light complexity level.[6] To overcome such

*This paper was recommended by Regional Editor Giuseppe Ferri.

issues, many researchers proposed design approaches with higher-dimensional chaotic systems.[7] Herein, it should be noted that if the designed chaotic systems possess the same number of positive Lyapunov exponent no matter what their number of dimensions, i.e., single, double and higher dimensional, their chaotic behaviors' complexity will be quite similar.[7] The systems with more than one positive Lyapunov exponents, i.e., hyperchaotic systems, offer more complexity for chaotic cryptosystems and communications. Hence, hyperchaotic systems' nonlinear dynamic behavior is more complicated and less predictable as compared to their chaotic counterpart, independent of their dimensions. The complexity increases in the carrier signal either by using memristor that provides initial condition sensitivity,[8,9] coexisting attractors[10,11] or image encryption algorithm[12] and produces many applications areas, e.g., fingerprint, image and cryptology.

In the design of chaotic signals, Cellular Neural Network (CNN) offers interchangeability among different nonlinear structures just by adjusting the system parameters in the dynamic equations. The most tedious limitation of CNN that stems from the existence of one nonlinear term in the dynamic equations has been handled with the presence of State Controlled-Cellular Neural Network (SC-CNN). The presence of more than one nonlinear term in the dynamic equations, however, appears as a challenge for the SC-CNN. All the efforts to enhance and increase the complexity of chaotic signals that give rise to unpredictability, hence safer communication, led researchers to come up with Switched State Controlled-Cellular Neural Network (Switched SC-CNN). Switched SC-CNN, however, cannot be activated with the *sgn* function and requires the use of error function series to create multi-scroll chaotic attractors that offer way more complexity than it is acquired with single-scroll attractors. To upgrade the behavior of chaotic attractors, e.g., single or multiple, to hyperchaos, one needs either an additional dynamic equation or a design of fractional-order with the aim of increasing the complexity of chaotic signals, hence providing safer and reliable communication. Unlike integer-order design, fractional-order design suffers from meticulous modeling process along with challenging calculation steps, but it gives higher modeling accuracy with enhanced complexity.[13]

Among the studies on chaotic oscillators, one of the most exciting aspects is to generate attractors with more than one scroll, i.e., n-scroll attractors. On the generation of multi-scroll attractors, the quasi-linear function approach was the first design idea. In 1991 and 1993, Suykens and Vandewalle introduced that piecewise linear (PWL) functions can be used in the generation of multi-scroll attractors.[14–16] In the following years, nonlinear modulating functions, e.g., trigonometric functions, adjustable wave function approaches, e.g., sawtooth or triangular, and nonlinear transconductor method were preferred more than PWL functions in the generation of multi-scroll attractors.[17] In addition to these functions, the Sine function for the generation of multi-scroll chaotic attractors was deputed in 2001 by Tang *et al.* and improved in 2003 by Cafagna and Grassi.[18–20] The use of nonlinear transconductor

Table 1. Related literature comparison.

Literature	Complexity of the system	Offset boosting method	Hardware implementations
Suykens and Vandewalle[14–16]	Multi-scroll	PWL	NO
Lü and Chen[17]	Multi-scroll	Trigonometric, adjustable wave, sawtooth, triangular function	NO
Tang *et al.*[18]	Multi-scroll	Sine function	NO
Cafagna and Grassi[19]	Multi-scroll and Hyperchaotic	Sine function	NO
Özoguz *et al.*[21]	scroll grid	Transconductor	NO
Yalçin *et al.*[23]	Multi-scroll and Hyperchaotic	State variable direction	NO
Günay and Altun[42]	Multi-scroll	tanh	YES (Analog)
This paper	Multi-scroll and Hyperchaotic	Erf function	YES (Analog)

method in the generation of multi-scroll attractors was first realized by Özoguz *et al.*[21] and Salama *et al.*[22] Yalçin *et al.* in 2002 used a step circuit design to create a set of scroll-grid chaotic attractors.[23] The main purpose behind the generation of multi-scroll chaotic structures is to increase the complexity in the chaos system. There are too many methods to enhance the complexity in the chaos system, and a multi-scroll structure is just one of them. The relevant literature comparison is shown in Table 1. According to Shilnikov,[24] nonlinear system's number of chaotic attractors and the number of equilibrium points are highly related. To observe the chaotic behavior in the system, there should be at least one unstable equilibrium point. To this end, it can be inferred that the increase in the number of scrolls can be acquired with the increase in the number of unstable equilibrium points. The way of offset boosting can be increased with the addition of polynomial, sawtooth, hyperbolic, *tanh*, step, etc., functions.[17,25,26] In this paper, offset boosting is provided with error function.

SC-CNN-based chaotic oscillators, among many autonomous chaos generators, draw a significant amount of attention because of their easier realization, i.e., inductorless design. It can be easily seen from the literature that a variety of chaotic circuits and complex dynamic systems are modeled and used in chaotic cryptography as well as secure communications as chaos generators in the development history of SC-CNN. In the evolution of CNNs, SC-CNN composes a vital step, in which SC-CNN has been used to create a prototype for complex dynamical systems. Various complex dynamical systems and chaotic circuits have been modeled and utilized in the realization of secure communications and chaotic cryptography.[27–38] It has been shown in several studies that SC-CNN can also be used in multi-scroll generation. The use of PWL characteristic in the output function of SC-CNN was presented by Arena *et al.* to show that multi-scrolls can be generated in SC-CNN[29]; n-double-scroll attractors were generated using hypercubes as used in single-dimensional (1D)

CNNs.[39] To be able to have multi-scrolls in SC-CNN, Günay and Altun proposed hyperbolic tangent function series.[40] In the case of nonlinearity in a function that has more than one variable, SC-CNN cell circuit's canonic PWL output function becomes inadequate. This limitation can be overcome through the use of Switched SC-CNN that can be used to imitate the nonlinear functions with more than one variable.[41,42] In these studies,[41,42] Rössler system, Sprott Case F and Lorenz system, which have quadratic-type nonlinearities, are modeled using Switched SC-CNN. The dynamic structure of the chaotic system can be enhanced with hyperchaotic modeling. Herein, the fractional-order modeling is one of the widely used methods to urge a dynamic system to exhibit hyperchaotic behavior.

In this paper, the fractional-order design in addition to switched SC-CNN is proposed as a modeling approximation to generate multi-scrolls, i.e., improve and increase the structure complexity. Chaotic systems that have enhanced dynamic features are more suitable for providing safer and reliable communication. The fractional-order systems increase the structure complexity as compared to integer-order systems due to better approximation of their system behavior to reality. Specifically, fractional-order system designs urge chaotic-based oscillators to exhibit hyperchaos. Hyperchaos behavior among chaotic dynamic systems is preferred in chaos-based applications, e.g., cryptology, reliable communication, embedded system and signal processing. To increase the complexity in the generation of pseudo-random number, and in the encryption of image, hyperbolic tangent-cubic nonlinear function, coexisting multiple attractors, transient period, intermittent chaos and offset boosting are proposed.[43–46] To this end, we propose a systematic design approach to generate multi-scroll attractors with hyperchaotic behavior using fractional-order systems, where switched SC-CNN is triggered with error function.

This paper is organized as follows. First, we mention about the Charef approximation method and give the derivation of fractional-orders. Later, Sprott Case H, which depicts the quadratic nonlinearity, is transferred to Switched SC-CNN version and then analyzed from the perspective of dynamical system behaviors. Theoretical analysis of the proposed system's dynamical behaviors is scrutinized, while numerical investigations are carried out with equilibrium points, Lyapunov exponent, bifurcation diagrams, Poincaré mapping and 0/1 test methods. Numerical results are also verified on an FPAA (Field Programmable Analog Array) platform. Finally, a discussion and conclusion parts are presented.

2. Fractional Calculus

Nonlinear functions cannot always exhibit chaotic behavior and require the third-order state equation to provide chaos condition. On the other hand, with the help of the nonlinear equations that are generated using fractional-order derivative operators, the third-order state equation is not required to provide chaos conditions. In such a case, chaotic behavior can be observed even in the case total order of the dynamic systems is < 3.[47] The nonlinear equations generated using fractional-order derivative operators, even with the order of < 3, can further increase the unpredictability of chaotic systems.[47]

The question of whether the meaning of an integer-order derivative can be generalized to noninteger orders led Leibniz and L'Hopital to introduce the fractional-order derivative with the order of 0.5.[48,49] In fact, this scholar's curiosity reveals that fractional calculus is indispensable to system modeling, especially for the control systems.[50–54] On the other hand, the calculation process of fractional-order is complicated, challenging and time-consuming. In general, to alleviate the difficulties of this process for analysis and simulations of control systems, the fractional-order operators are rounded to the closest integer-order transfer functions with the cost of sacrificing the modeling accuracy. To calculate fractional-order derivative with better approximation of complete system behavior, an additional parameter is used as an interpolation between neighboring integer derivatives. Hence, nonlinear systems can be modeled with higher fidelity and accuracy. To this end, a great deal of effort has been put by researchers to introduce a variety of methods, e.g., Grünwald–Letnikov's (GL), Riemann–Liouville (RL) and the Charef approximation, to better approximate fractional-order operators to the integer-order transfer functions.[55]

The calculation of fractional-order can be defined as (1). Herein, complex derivative or integral order is defined with α.

$$
{}_aD_x^\alpha = \begin{cases} \dfrac{d^\alpha}{dt^\alpha}; & \mathrm{Re}(\alpha) > 0\,, \\ 1; & \mathrm{Re}(\alpha) = 0\,, \\ \displaystyle\int_a^t (d\tau)^{-\alpha}; & \mathrm{Re}(\alpha) < 0\,. \end{cases} \tag{1}
$$

Among the definition of fractional-order systems, the Charef approximation method is preferred in this study, and its brief explanation is given in the following subsection.

The Charef Approximation Method

In the field of fractional analysis, the Charef approximation approach is known as the widely used definition.[56] Based on the Charef approximation approach definition, the mathematical expression of fractional-order integral equation (2) is given as

$$
I^\alpha{}_{(s)} = \frac{1}{s^\alpha}\,, \tag{2}
$$

where $s = j\omega$ and α stand for complex frequency and order of positive fractional integrator.

$$
I^\alpha{}_{(s)} = \frac{1}{s^\alpha} \approx \frac{1}{\left(1 + \dfrac{s}{p_T}\right)^\alpha}\,, \quad 0 < \alpha < 1\,, \tag{3}
$$

where p_T refers to corner frequency. To this end, the fractional-order transfer function can be described as

$$I^{\alpha}{}_{(s)} = \frac{1}{s^{\alpha}} \approx \frac{1}{\left(1 + \dfrac{s}{p_T}\right)^{\alpha}} \lim_{N\to\infty} \frac{\prod_{i=0}^{N-1}\left(1 + \dfrac{s}{z_i}\right)}{\prod_{i=0}^{N}\left(1 + \dfrac{s}{p_i}\right)}\,. \tag{4}$$

The transfer function given in (4) helps to calculate the poles and zeros of a given dynamic system in (5).

$$\begin{aligned} p_0 &= p_T 10^{[y/20\alpha]}, \quad z_0 = p_0 10^{[y/10(1-\alpha)]}\,, \\ p_1 &= z_0 10^{[y/10\alpha]}, \quad z_1 = p_1 10^{[y/10(1-\alpha)]}\,. \end{aligned} \tag{5}$$

In these equations, corner frequency, first pole value and error rate in dB are defined with p_T, p_0 and y in the calculation of the approximated transfer function, respectively. $1/p_T$ stands for the time constant of relaxation.

Equation (6) describes the $N-1$ zero and N pole ratio.

$$z_{N-1} = p_{N-1} 10^{[y/10(1-\alpha)]}, \quad p_N = z_{N-1} 10^{[y/10\alpha]}\,. \tag{6}$$

N helps determining the last pole value, p_N. Equation (7) provides the values of a, b and ab that express the $N-1$ pole and N zero ratio.

$$a = 10^{[y/10(1-\alpha)]}, \quad b = 10^{[y/10\alpha]}, \quad ab = 10^{[y/10\alpha(1-\alpha)]}\,. \tag{7}$$

These explanations help us derive the equation for the transfer function as

$$I^{\alpha}{}_{(s)} = \frac{1}{s^{\alpha}} \approx \frac{1}{\left(1 + \dfrac{s}{p_T}\right)^{\alpha}} \approx \frac{\prod_{i=0}^{N-1}\left(1 + \dfrac{s}{z_i}\right)}{\prod_{i=0}^{N}\left(1 + \dfrac{s}{p_i}\right)} = \frac{\prod_{i=0}^{N-1}\left(1 + \dfrac{s}{(ab)^i a p_0}\right)}{\prod_{i=0}^{N}\left(1 + \dfrac{s}{(ab)^i p_0}\right)}\,. \tag{8}$$

Moreover, the dimension of the transfer function, N, can be found as

$$N = \mathrm{int}\left(\frac{\log\left(\dfrac{\omega_{\max}}{p_0}\right)}{\log(ab)}\right) + 1\,. \tag{9}$$

In the conclusion of Eqs. (8) and (9), s^{α} value, within the interval of specific frequency and error rate, can be approximately obtained in the frequency domain with the Charef approximation method. The Charef approximation implies the integral calculation for the given function where the fractional-order derivative is acquired with fractional-order integral and integer-order derivatives.

As it is discussed before, at least the third-order dynamic representation is needed to express chaotic systems in the case that conventional calculation methods are preferred. On the other hand, to model a chaotic system with fractional-order system approximation, the fractional-order derivative is utilized. In this study, the Charef approximation approach is chosen in the frequency domain expression of fractional-order for MATLAB Simulink and analog-based FPAA.[57] The Charef approximation is the most suitable method as it allows to obtain a continuous approximation of fractional-order system in s-domain[55] among frequency domain modeling definition. With the help of this method, approximated integer-order transfer function of fractional-order integral can be achieved within the specific interval of frequency and error rate.[58] Furthermore, to realize the proposed method in FPAA hardware, the requirement of FPAA structures to be designed in frequency domain led to the use of the Charef approximation method. The transfer function obtained with the Charef approximation method can be easily integrated into numerical simulations and FPAA implementations. Sprott type-H chaotic system' fractional-order transfer function in frequency domain is acquired to, respectively, implement in Simulink and FPAA. Using the selected, minimum fraction-order, the dynamic system's eigenvalues are calculated to determine transfer function. Equation (10) shows how to determine fraction-order for every eigenvalue. The fraction-order of the system is identified with the selection of the greatest value among the obtained fraction-order.[59] Jacobian matrices obtained for each dimension of the given dynamic system are used to identify eigenvalues, $(\lambda_1, \lambda_2, \ldots, \lambda_n)$. Then, the fraction order, α, can be calculated with the help of obtained eigenvalues as shown in (10), where q refers to the determined fraction order.

$$|\arg(\lambda_i)| > \alpha\pi/2, \quad \alpha = \max(q_1, q_2, \ldots, q_n), \quad \forall(i = 1, 2, \ldots, n)\,. \tag{10}$$

The stability of a system implies that fractional-order system lies at a stable point. In the case that the given system implies unstability, the chaos exhibition can appear in the fractional-order system. The fractional-order systems' stability theorem is summarized in Fig. 1.

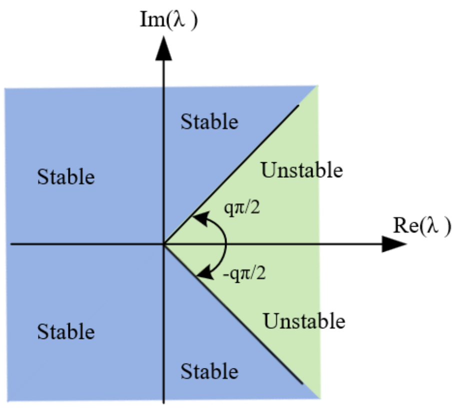

Fig. 1. Stability region of the fractional-order system.

$\lambda_1 = -1$, $\lambda_2 = 0.25 + i0.968246$ and $\lambda_3 = 0.25 - i0.968246$ are the eigenvalues of Sprott type-H chaotic system's Jacobian matrix for the given initial conditions and parameters. Using the corresponding eigenvalues, the fraction-orders need to be determined are obtained as follows: $\arg(\lambda_1) = \pi$, $\arg(\lambda_2) = 1.31812$ and $\arg(\lambda_3) = -1.31812$. Upon determining the fraction-orders with the help of the expression $\max(q_1, q_2, q_3)$, it can be found as follows: $\alpha = q_2 = q_3 = 0.9377$. Herein, if $q_i \geq 0.9377$ for every $i = 1, 2, 3$, then all the equilibrium of Eq. (10) lies at the region of unstability that may lead the dynamic system to exhibit possibly chaos. Lyapunov exponents of the proposed system are given as $L_1 = 0.0855$, $L_2 = 0.0743$ and $L_3 = -0.6298$.[60] Hyperchaos is first defined as a system with more than one positive Lyapunov exponent in the classical example of hyperchaotic systems paper, written by Rossler in 1979.[13] Hyperchaotic system has many positive Lyapunov exponents, which means that the motion of the system extends in many directions, so the hyperchaotic system has stronger randomness and unpredictability than the general chaotic system.[61–64]

$$H(s) = \frac{\mathrm{num}(s)}{\mathrm{den}(s)} = \frac{1.377s + 3.793}{s^2 + 4.494s + 0.0057}\,. \tag{11}$$

The transfer function obtained in Eq. (11) represents the fraction order, $\alpha = 0.94$, in frequency domain and is used to design Simulink and FPAA CAM (Configurable Analog Module).

This section was devoted to explain the chaotic system's remodeling with fraction-order method, which offers a closer approximation to the real system's behavior. In the following section, CNN-based design of dynamic equations that include the second-order nonlinear terms will be clarified. Switched SC-CNN design by transforming variables will be articulated for realizing the CNN model of dynamic equations that include the second-order nonlinear terms. With this method, CNN-based design of dynamic systems paves the way for faster calculation and integrated structure that has higher processing capacity.

3. Switched SC-CNN-Based Chaotic Systems

As we emphasized earlier in the paper, switched-SC-CNN approach can be defined with nonlinear state equations that are dimensionless given as follows[40]:

$$\begin{aligned} \dot{x}_j &= -x_j + a_j y_j + G_o + G_s + G_n + i_j\,, \\ y_j &= \frac{1}{2}\left[|x_j + 1| - |x_j - 1|\right]. \end{aligned} \tag{12}$$

In Eq. (12), while state variables are represented by x_j, outputs are given by y_j. i_j and a_j, respectively, are referred to as thresholds and feedback from the outputs of neighbor cells in SC-CNN. G_s and G_o denote the linear combinations of the outputs and state variables, respectively. G_n represents the bipolar voltage controlled switching parameters that surrogate the state variables' possible quadratic variations. For three connected cells, Eq. (13) gives the generalized Switched SC-CNN as

$$\begin{aligned}
\dot{x}_1 &= -x_1 + \sum_{k=1}^{3} a_{1k} y_k + \sum_{k=1}^{3} s_{1k} x_k + \sum_{k=1}^{3} n_{1k} x_k + i_1 \,, \\
\dot{x}_2 &= -x_2 + \sum_{k=1}^{3} a_{2k} y_k + \sum_{k=1}^{3} s_{2k} x_k + \sum_{k=1}^{3} n_{2k} x_k + i_2 \,, \\
\dot{x}_3 &= -x_3 + \sum_{k=1}^{3} a_{3k} y_k + \sum_{k=1}^{3} s_{3k} x_k + \sum_{k=1}^{3} n_{3k} x_k + i_3 \,.
\end{aligned} \tag{13}$$

In Eq. (13), state variables are denoted by x_i for every $i = 1, 2, 3$, and the outputs can be represented with y_k. The feedback from the outputs and the states of the neighbor cells are given with a_k and s_k, respectively. The thresholds of the cells are described with i_i for every $i = 1, 2, 3$. The switching parameters that are changing with cells' output conditions, i.e., y_k in Eq. (14), are given with n_k.

The PWL output function of CNN, SC-CNN and Switched SC-CNN is depicted in Fig. 2.

$$\begin{aligned}
n_k &= \begin{cases} 1 \,, & (y_k \pm i_k) \geq 0 \,, \\ -1 \,, & (y_k \pm i_k) < 0 \,, \end{cases} \\
y_k &= \frac{1}{2}\left[|x_k + 1| - |x_k - 1|\right].
\end{aligned} \tag{14}$$

The Sprott Case H system's state variables are denoted as follows[65]:

$$\begin{aligned}
\dot{x} &= -y + z^2 \,, \\
\dot{y} &= x + ay \,, \\
\dot{z} &= x - z.
\end{aligned} \tag{15}$$

For initial values (0.1, 0.1, 0), the Lyapunov exponents based on the original equation structure of the Sprott H system are given as $L_1 = 0.081548$, $L_2 = -0.005678$ and $L_3 = -0.575870$ and are shown in Fig. 5. The state variables

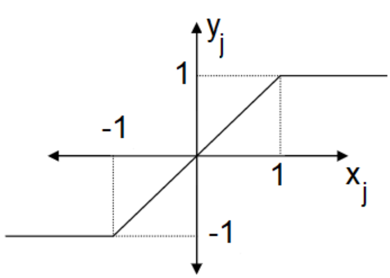

Fig. 2. PWL output function of CNN, SC-CNN and Switched SC-CNN.

given in (15) can be transformed using (13) to a switched SC-CNN structure given as follows:

$$\begin{aligned}
&\dot{x}_1 \pm = -x_1 + s_{11}x_1 + s_{12}x_2 + n_{13}(y_3 + i_3) + i_3^2\,,\\
&\dot{x}_2 = -x_2 + s_{21}x_1 + s_{22}x_2\,,\\
&\dot{x}_3 = -x_3 + s_{31}x_1\,,\\
&y_3 = \frac{1}{2}[|x_3 + 1| - |x_3 - 1|]\,,\\
&x = x_1, \quad y = x_2, \quad z = x_3, \quad a = s_{22}, \quad s_{12} = -1, \quad s_{11} = s_{21} = s_{31} = i_3 = 1\,,\\
&s_{13} = s_{23} = s_{32} = s_{33} = 0; \quad i_1 = i_2 = 0\,,\\
&n_{11} = n_{12} = n_{21} = n_{22} = n_{23} = n_{31} = n_{32} = n_{33} = 0\,,\\
&a_{11} = a_{12} = a_{13} = a_{21} = a_{22} = a_{23} = a_{31} = a_{32} = a_{33} = 0\,,\\
&n_{13} = \begin{cases} +1; & (y_3 - i_3) \geq 0\,,\\ -1; & (y_3 - i_3) < 0\,. \end{cases}
\end{aligned} \tag{16}$$

The nonlinearity in the Sprott Case H system is obtained by quadratic z^2 function as depicted in (15). The same nonlinearity in Switched SC-CNN system can be acquired provided that $z^2 = y_3^2 = (y_3 + i_3)(y_3 - i_3) + i_3^2$. Here, i_3 equals to a constant. $n_{13}(y_3 + i_3)$ is used instead of the product of $(y_3 + i_3)(y_3 - i_3)$, and n_{13} surrogates to $\mathrm{sgn}(y_3 - i_3)$.

Remark 1. For $\dot{x}_1$, the parameter n_{13} acts like a switch at a zero threshold level and creates two different occasions:

- When $(y_3 - i_3)$ is positive, n_{13} is equal to 1 (switch > 0),
- When $(y_3 - i_3)$ is negative, n_{13} is equal to -1 (switch < 0).

With using the conditions and variables given in Remark 1, state equations obtained with the switching of the dynamic system that include the second-order nonlinear terms are given in Eq. (17). These two occasions can be mathematically expressed as

$$\begin{aligned}
&\dot{x}_1 + = -x_1 + s_{11}x_1 + s_{12}x_2 + n_{13}(y_3 + i_3) + i_3^2, \quad (y_3 - i_3) \geq 0\,,\\
&\dot{x}_1 - = -x_1 + s_{11}x_1 + s_{12}x_2 - n_{13}(y_3 + i_3) + i_3^2, \quad (y_3 - i_3) < 0\,.
\end{aligned} \tag{17}$$

4. Discussions for Stability and Numerical Results of Switched State Controlled-CNN-Based Sprott Case H

Determining the chaos conditions of the Sprott H system has been carried out using Switched SC-CNN and realizing numerical analysis for both switching states to select accurate parameters under the given conditions. This section provides information about how to select accurate parameters for generating a multi-scroll chaotic attractor with Switched SC-CNN.

The equilibrium points of Eq. (16) are represented in two subspaces where D_+ and D_-, respectively, refer to subspaces when x_3 is positive and negative and can be given as follows:

$$\begin{aligned} D_+ &= \{(x_1, x_2, x_3) | x_3 \geq 0\} : P^+ = (-k_1, -k_2, -k_3) \\ D_- &= \{(x_1, x_2, x_3) | x_3 < 0\} : P^- = (k_1, k_2, k_3)\,. \end{aligned} \tag{18}$$

for $n_{13} = \pm 1$, where

$$\begin{aligned} k_1 &= \frac{-(i_3 - i_3 s_{22})}{(s_{11} + s_{22} + s_{31} - s_{11}s_{22} + s_{12}s_{21} - s_{22}s_{31} - 1)}\,, \\ k_2 &= \frac{(-i_3 s_{21})}{(s_{11} + s_{22} + s_{31} - s_{11}s_{22} + s_{12}s_{21} - s_{22}s_{31} - 1)}\,, \\ k_3 &= \frac{(i_3 s_{31}(s_{22} - 1))}{(s_{11} + s_{22} + s_{31} - s_{11}s_{22} + s_{12}s_{21} - s_{22}s_{31} - 1)}\,. \end{aligned}$$

In regions D_+ and D_-, Eq. (18) is linear where its equilibrium points, P^+ and P^-, are derived using the system's *Jacobian matrices*:

$$J_\pm = \begin{vmatrix} (s_{11} - 1), & s_{12}, & 1 \\ s_{21}, & (s_{22} - 1), & 0 \\ s_{31}, & 0, & -1 \end{vmatrix}. \tag{19}$$

After getting equilibrium points, P^+ and P^-, we can find the characteristic equation of the given system as

$$\begin{aligned} S(\lambda) = \lambda^3 + (3 - s_{11} - s_{22})\lambda^2 + (3 - 2s_{11} - 2s_{22} + s_{11}s_{22} - s_{12}s_{21})\lambda + s_{11}s_{22} \\ - s_{12}s_{21} + 1\,. \end{aligned}$$

To find system's equilibrium points with eigenvalues, the parameter values, $s_{11} = s_{21} = s_{31} = 1; s_{12} = -1; s_{22} = 1.3; i_3 = 0.1$, and the initial conditions $(0.1, 0.1, 0)$ are substituted in the system's *Jacobian matrices* as shown in Eq. (19). Accordingly, the calculated eigenvalues and equilibrium points of the system are given in Table 2.

Remark 2. Proposed Switched SC-CNN system refers to an unstable operation, where the equilibrium S settles at saddle-focus.

- When $n_{13} = 1$, λ_1, and λ_2 with λ_3, respectively, refer to negative real number, and complex conjugate eigenvalues with positive real parts.

Table 2.

n_{13}	x_1	x_2	x_3	λ_1	λ_2	λ_3
1	0.0769	−0.0231	−0.0231	−1.4884	0.3942+0.8474i	0.3942 − 0.8474i
−1	0.1428	−0.0428	−0.0428	−0.4414	−0.1293+1.2572i	−0.1293 −1.2572i

Remark 3. Proposed Switched SC-CNN system refers to a stable operation, where the equilibrium S settles at focus node.

- When $n_{13} = -1$, λ_1, and λ_2 with λ_3, respectively, refer to negative real number, and complex conjugate eigenvalues with positive real parts.

In Figs. 3(a)–3(h), the coexistence of different attractors at each step from period-2 limit cycle to chaos are presented.

In the positive switching condition given in Remark 2, time-series and phase-space demonstrations, including 2T and 4T periodic windows, for the two different values of constant parameter, $i_3 = 1.68$ and $i_3 = 1.72$, are depicted in Figs. 3(a)–3(d). In the negative switching condition given in Remark 3, time-series and phase-space demonstrations, including 2T and 4T periodic windows, for the two different values of constant parameter, $i_3 = -1.68$ and $i_3 = -1.72$, are given in Figs. 3(e)–3(h). In addition to these, time-series and phase-space illustration of the system's chaotic behavior obtained for $i_3 = 0.3$ is given in Figs. 3(i) and 3(j).

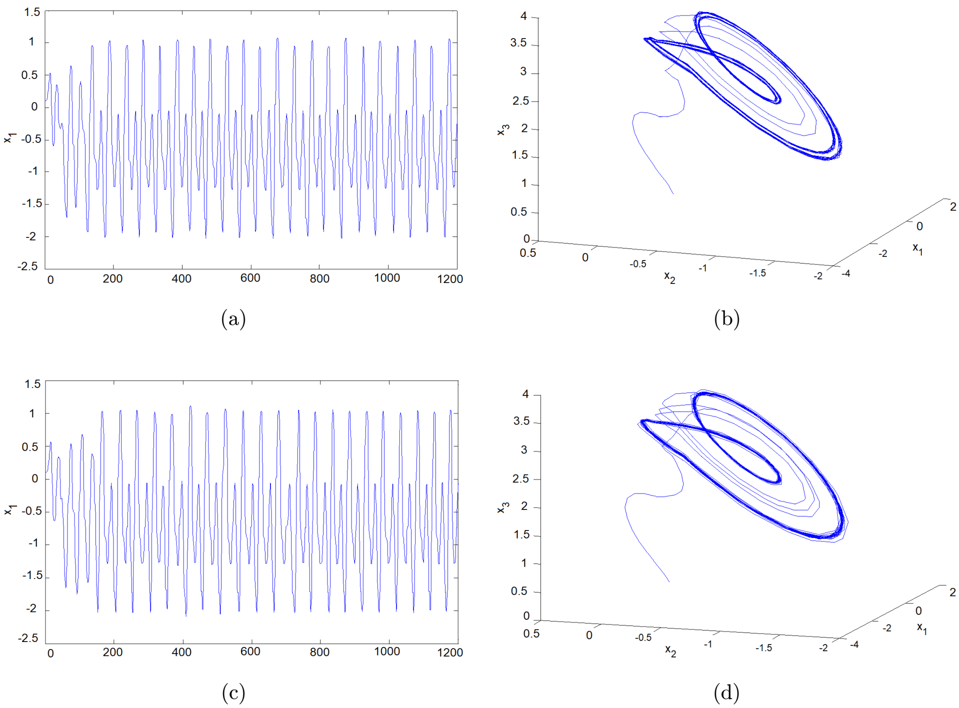

Fig. 3. (a) Time series of $x_1(t)$ dynamic for $i_3 = 1.68$, (b) 4T-periodic solution for $i_3 = 1.68$, (c) time series of $x_1(t)$ dynamic for $i_3 = 1.72$, (d) 2T-periodic solution for $i_3 = 1.72$, (e) time series of $x_1(t)$ dynamic for $i_3 = -1.72$, (f) 2T-periodic solution for $i_3 = -1.72$, (g) time series of $x_1(t)$ dynamic for $i_3 = -1.68$, (h) 4T-periodic solution for $i_3 = -1.68$, (i) time series of $x_1(t)$ dynamic for $i_3 = 0.3$ and (j) chaotic solution for $i_3 = 0.3$.

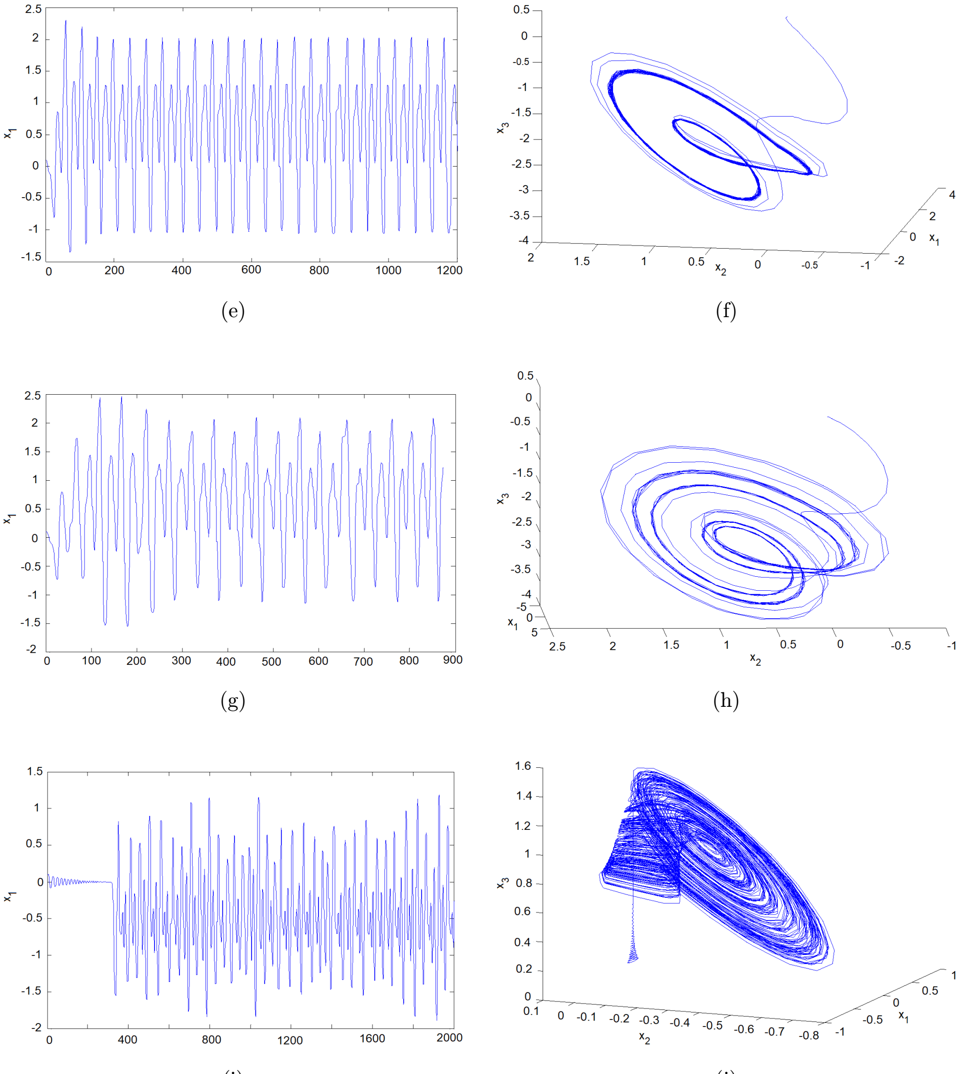

(e) (f)

(g) (h)

(i) (j)

Fig. 3. (*Continued*)

Herein, we carry out two different bifurcation observations: the values, $i_3 = 0.3$ and $s_{22} = 1.3$, where the system exhibits chaotic behavior, are distinctly kept fixed to obtain parameter's bifurcation diagrams. (i) the system parameters are set to $s_{11} = s_{21} = s_{31} = 1$; $s_{12} = -1$; $i_3 = 0.3$, while s_{22} is varying, (ii) the system parameters are set to $s_{11} = s_{21} = s_{31} = 1$; $s_{12} = -1$; $s_{22} = 1.3$, while i_3 is varying. These bifurcation diagrams' time-series and phase-space demonstrations are given in Figs. 3(a) and 3(j). In (i), the system's numerical calculation with $s_{22}\varepsilon$ [0.3,0.4] for an increment

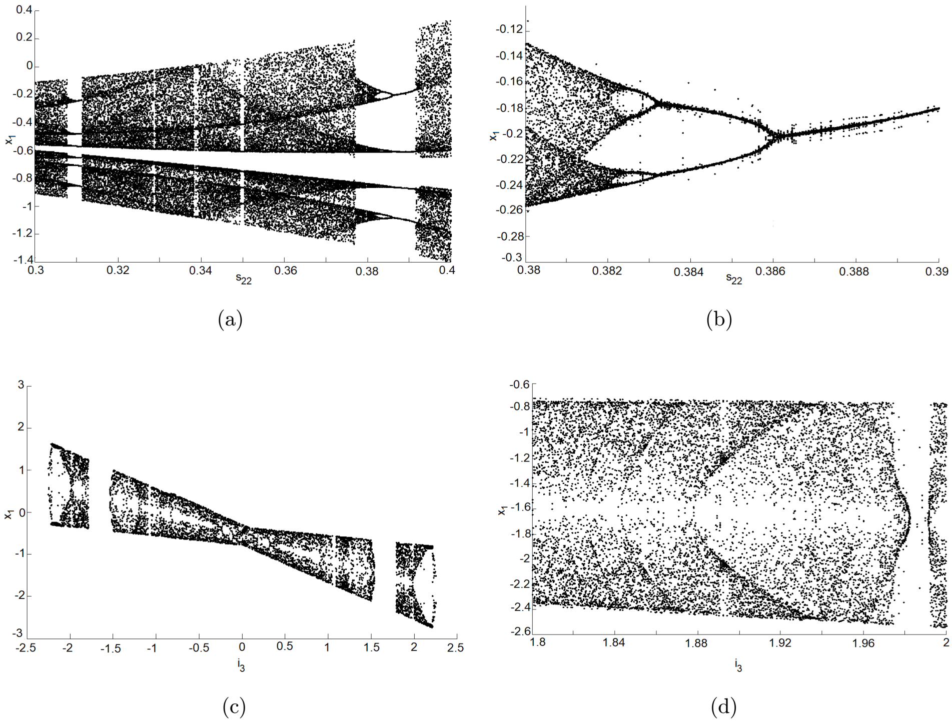

Fig. 4. (a) Bifurcation diagrams with x_1 versus $s_{22} \in [0.3, 0.4]$ for an increment of $\Delta s_{22} = 0.001$, (b) pitchfork bifurcation occur at $s_{22} \in [0.382, 0.386]$, (c) bifurcation diagrams with x_1 versus $i_3 \in [-2.5, 2.5]$ for an increment of $\Delta i_3 = 0.001$ and (d) periodic and chaotic sequences for $i_3 \in [1.8, 2]$.

of $\Delta s_{22} = 0.001$ is carried out. The bifurcation diagram is shown in Figs. 4(a) and 4(b). Pitchfork bifurcations occur at $s_{22}\varepsilon$ [0.307, 0.312] and $s_{22}\varepsilon$ [0.382, 0.386]. In (ii), the system is simulated numerically with $i_3\varepsilon$ [−2.5, 2.5] for an increment of $\Delta i_3 = 0.001$. Besides periodic windows, the bifurcation diagrams including chaotic regions are shown in Figs. 4(c) and 4(d).

The systems' Lyapunov exponents variations are numerically computed in the axis of $i_3 \in [-2.5, 2.5]$ and $s_{22} \in [0, 0.45]$ with the increments of $\Delta s_{22} = 0.01$ and $\Delta i_3 = 0.01$. This computation takes 106 iterations using the Runge–Kutta algorithm in the fourth order, and the graphics that are obtained from the calculations of Lyapunov exponents variations are shown in Fig. 5.

When the Lyapunov analysis is carried out for i_3, and s_{22} similar to the previous analysis, it is observed that the same results are obtained for given intervals. The Lyapunov exponents calculated for the varying values of i_3 are shown in Fig. 5(a). It can be observed here that the maximum Lyapunov exponent is acquired for the value of $i_3 = 0.3$. For the varying values of s_{22}, the Lyapunov exponents are depicted in Fig. 5(b), where Lyapunov exponents reach to their maximum for $s_{22} = 0$–0.45.

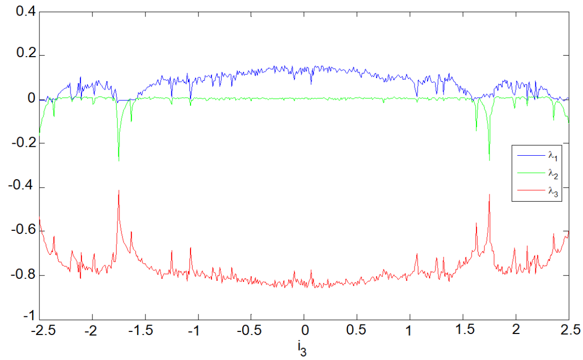

(a)

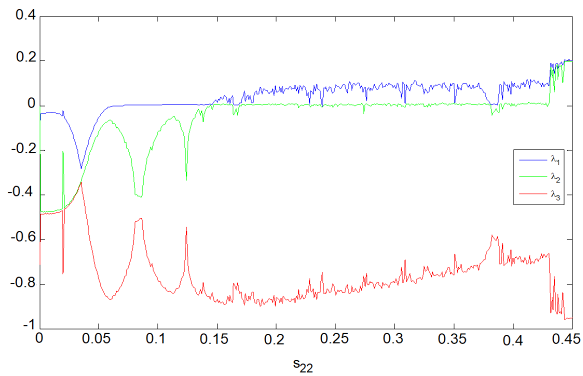

(b)

Fig. 5. Lyapunov exponents of the system for (a) varying $i_3 \in [-2.5, 2.5]$ and (b) varying $s_{22} \in [0, 0.45]$.

The one-to-one correspondence of bifurcation diagram with the exponential spectrum is illustrated in Fig. 6. In this figure, the values of Lyapunov exponents for the varying i_3 and bifurcation diagram with chaotic–periodic windows can be observed. The initiation of chaotic–periodic window starts when the value of switching parameter becomes around $i_3 = -2.3$ for which one of the Lyapunov exponents is turning to the positive value. The presence of chaotic window continues as long as at least one of the Lyapunov exponents remains positive. For the values of the switching parameter from -1.72 to -1.68, i.e., $i_3 = [-1.72, -1.68]$, all the Lyapunov exponents become negative, and all the chaotic windows are simultaneously disappeared. Similar to the previous case, when the value of the switching parameter becomes around $i_3 = [-1.68, 1.68]$, chaotic windows appear again with one positive Lyapunov exponent. Once again, for the values of switching parameter from 1.68 to 1.72, i.e., $i_3 = [1.68, 1.72]$, all the Lyapunov exponents become negative, and all the chaotic windows simultaneously disappear.

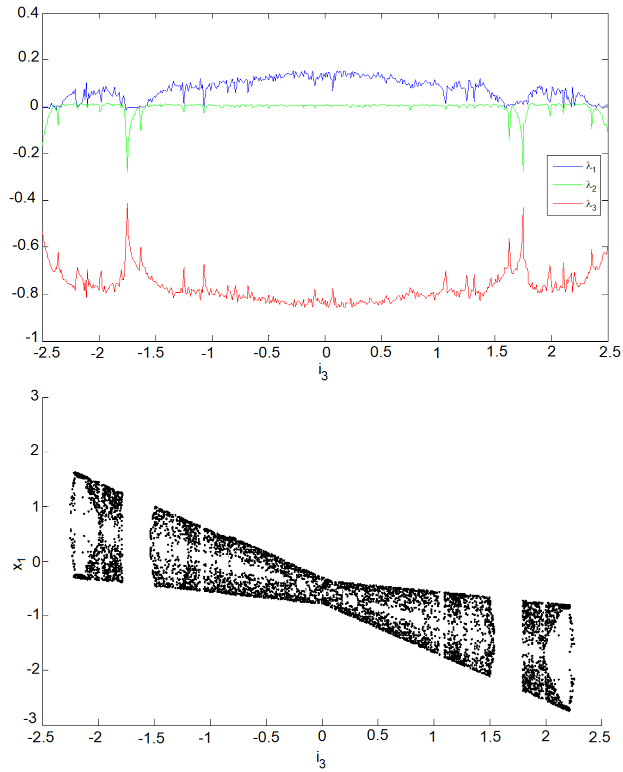

Fig. 6. Bifurcation diagram of x_1 and Lyapunov exponent spectrum with i_3 increasing.

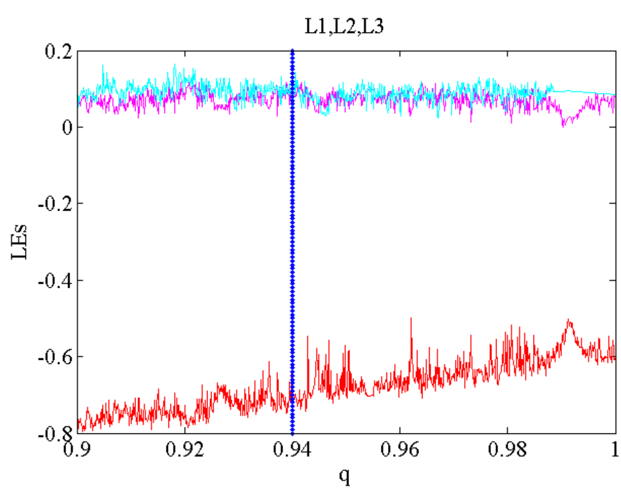

Fig. 7. Lyapunov exponents of the Sprott system case H when the fractional-order is 0.94, i.e., $q = 0.94$.

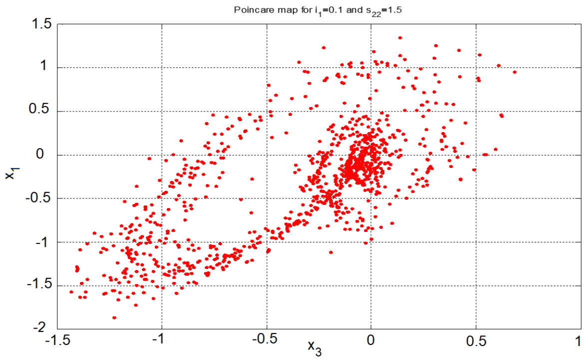

Fig. 8. The proposed system's Poincaré mapping for $i_1 = 0.1$ and $s_{22} = 1.5$.

In the second section of this paper, the minimum fraction value of the proposed fractional-order design is calculated as 0.94, i.e., $q = 0.94$, Lyapunov exponents of the Sprott system case H is also derived and two positive exponents are found as shown in Fig. 7. As a well-known fact, the hyperchaos is defined as a system with more than one positive Lyapunov exponents.[13] Lyapunov exponents of the proposed system are given as $L_1 = 0.0855$, $L_2 = 0.0743$ and $L_3 = -0.6298$, and its plot is illustrated in Fig. 7. These two positive exponents pose a system to exhibit hyperchaotic behavior.

For $i_1 = 0.1$ and $s_{22} = 1.5$ in $x_1(t) - x_3(t)$ domain, the proposed system's Poincaré mapping can be seen in Fig. 8. When we analyze the Poincaré mapping, which is attained for the variable values causing chaos condition obtained from the phase-space demonstration, bifurcation diagram and Lyapunov exponent given above, the selected plane, $i_1 = 0.1$ and $s_{22} = 1.5$, is intersected with many points. This situation once again verifies the existence of chaos for the proposed system.

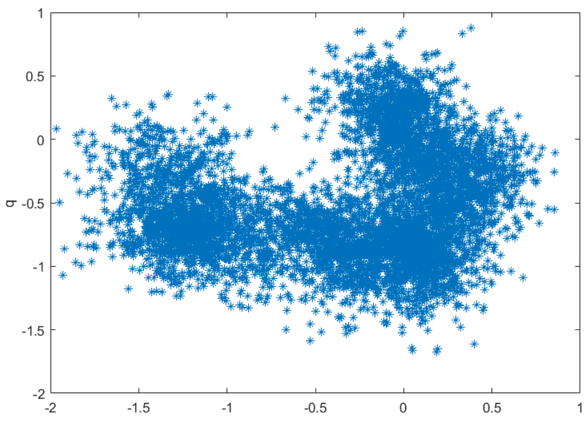

Fig. 9. 0/1 Test results of the proposed system for x_1 state variable.

Finally, we can once again confirm the appearance of the system's chaos conditions when we examine the p–q phase-space demonstration for x_1 state variable determined in chaos moment in Fig. 9. Here, we have utilized 0/1 test for the proposed system to observe whether the system exhibits chaotic behavior, and it is visualized in Fig. 9. In fact, 0/1 test is a chaos analysis method that can calculate nonlinear system behavior, in which it uses data output of a system without system equations.[66] With the help of this 0/1 test, we realize chaos analysis by evaluating the outcomes of calculated p–q iteration variables' phase-space exhibition. With this method, we can observe the generations of linear and nonlinear patterns in periodic signals and chaos conditions, respectively. Figure 9 depicts a sample of nonlinear patterns, where the system exhibits chaotic behavior.

5. Generation of Multi-Scroll Chaotic Attractors

In this section, first, the procedures of multi-scroll generation in fractional-order Switched SC-CNN-Based Sprott Case H system via error function series for $\alpha = q_1 = q_2 = q_3 = 0.94$ are presented. By using one-error function and two-error function series, many multi-scroll generators can be obtained. A chaotic system that has the fraction-order of $q = 0.94$ and total order of 2.82 is used with different output functions y_i, where $(i = 1, 2, 3)$, using error function to attain multi-scroll attractor. In case I, y_3 output function is used for switching in x_1 state variable to obtain multi-scroll attractor. In the remaining part of this study, multi-scroll attractors are attained for the given system dynamics with two-error function. In case II, y_3 output function is used for switching in x_1 state variable, while y_2 output function is used for switching in x_3 state variable to obtain multi-scroll attractor. In the subsections of this part, we present numeric analysis, simulations and FPAA implementations of these cases.

In the design of Switched SC-CNN, switching parameter n_{13} can be modeled with the sgn function. However, the nondifferentiability of the sgn function force designer to replace it with its continuous and differentiable equivalent[67] is as

$$\mathrm{sgn}(x) \Rightarrow \mathrm{erf}(kx)\,.$$

Herein, the error function, which can approximate the nonlinear dynamic behavior with a quite high accuracy,[68] is integrated into switched SC-CNN for the first time in the literature. The error function shows better accuracy than other widely used functions *tanh* that confirms in Fig. 10. Another considerable feature of error function is its differentiability, e.g., nonlinear characteristics of the sgn function prevent solving switching problems.[67,69] To this end, this paper aims to create a carrier signal that is highly unpredictable, in which multi-scroll attractors are acquired with the help of increased equilibrium points as the conclusion of error function usage in Sprott-H chaotic oscillators.

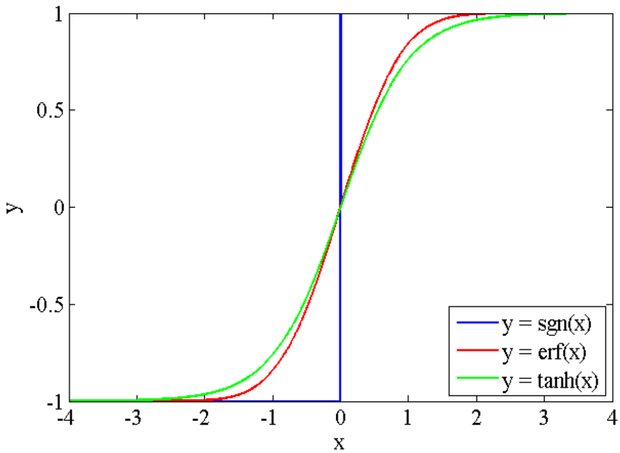

Fig. 10. Comparison of the tanh, erf and sgn functions.

Here, k is set such that error function is approximated to the sgn function. Hence, system's calculated Lyapunov exponent turns out to be independent of k. In this study, we first replace the sgn function with erf and set k to 100.

A. Using 1 — Error Function in Fractional-Order Switched SC-CNN-Based Sprott Case H system

Case I: y_3 output function is used for switching in x_1 state variable to obtain multi-scroll attractor.

Consider the following system:

$$\begin{aligned}
&D_t^{q1} x_1 \pm = -x_1 + s_{11}x_1 + s_{12}x_2 + [-\mathrm{erf}(ky_3) \pm i_3]\,,\\
&D_t^{q2} x_2 = -x_2 + s_{21}x_1 + s_{22}x_2\,,\\
&D_t^{q3} x_3 = -x_3 + s_{31}x_1\,,\\
&D_t^{q1} x_1 + = -x_1 + s_{11}x_1 + s_{12}x_2 + [-\mathrm{erf}(ky_3) + i_3]; \quad (\mathrm{switch} > 0)\,,\\
&D_t^{q1} x_1 - = -x_1 + s_{11}x_1 + s_{12}x_2 + [-\mathrm{erf}(ky_3) - i_3]; \quad (\mathrm{switch} < 0)\,,\\
&x = x_1, y = x_2, z = x_3\,,\\
&s_{11} = s_{21} = s_{31} = 1; s_{12} = -1; s_{22} = 1.3; i_3 = 0.2; k = 100\,,\\
&s_{13} = s_{23} = s_{32} = s_{33} = 0, i_1 = i_2 = 0\,,\\
&a_{11} = a_{12} = a_{13} = a_{21} = a_{22} = a_{23} = a_{31} = a_{32} = a_{33} = 0\,.
\end{aligned} \tag{20}$$

The equilibrium points of Eq. (20) exist in two subspaces defined as follows. Let D_1 be the subspace, where x_3 is positive, and D_2 be the subspace, where x_3 is negative:

$$\begin{aligned}
D_1 &= \{(x_1, x_2, x_3) | x_3 \geq 0\} : P_1 = (-a_1, -a_2, -a_3)\,,\\
D_2 &= \{(x_1, x_2, x_3) | x_3 < 0\} : P_2 = (a_1, a_2, a_3)\,,
\end{aligned} \tag{21}$$

where a_1, a_2 and a_3 are given as

$$a_1 = \frac{-(i_3 - i_3 s_{22})}{(s_{11} + s_{22} - k s_{31} - s_{11} s_{22} + s_{12} s_{21} + k s_{22} s_{31} - 2)}\,,$$
$$a_2 = \frac{-(i_3 s_{21})}{(s_{11} + s_{22} - k s_{31} - s_{11} s_{22} + s_{12} s_{21} + k s_{22} s_{31} - 2)}\,,$$
$$a_3 = \frac{(i_3 s_{31}(s_{22} - 1))}{(s_{11} + s_{22} - k s_{31} - s_{11} s_{22} + s_{12} s_{21} + k s_{22} s_{31} - 2)}\,.$$

In regions D_1 and D_2, Eq. (21) is linear, where its equilibrium points, P^1 and P^2, are derived using the system's *Jacobian matrices*:

$$J_{1,2} = \begin{vmatrix} (s_{11} - 1), & s_{12}, & 1 \\ s_{21}, & (s_{22} - 1), & 0 \\ s_{31}, & 0, & -1 \end{vmatrix}. \tag{22}$$

The characteristic equation of the system is given by

$$\begin{aligned} S_1(\lambda) = \lambda^3 + (3 - s_{11} - s_{22})\lambda^2 + (3 - 2s_{11} - 2s_{22} + s_{11} s_{22} - s_{12} s_{21})\lambda \\ - s_{11} - s_{22} + s_{31} + s_{11} s_{22} - s_{12} s_{21} - s_{22} s_{31} + 1\,, \end{aligned}$$

where the parameter values are

$$\begin{aligned} &s_{11} = s_{21} = s_{31} = 1; \quad s_{12} = -1; \quad s_{22} = 1.3; \quad i_3 = 0.2; \quad k = 100\,, \\ &s_{13} = s_{23} = s_{32} = s_{33} = 0, \quad i_1 = i_2 = 0\,, \\ &a_{11} = a_{12} = a_{13} = a_{21} = a_{22} = a_{23} = a_{31} = a_{32} = a_{33} = 0\,. \end{aligned}$$

Remark 4. System presented in Eq. (23) can generate multi-scroll chaotic attractors by utilizing the circumstances given as follows:

- Adding erf function in x_1 via y_3 nonlinearity;
- Parameters s_{11}, s_{12}, s_{21}, s_{22}, s_{31} satisfy conditions given in Eq. (20).

$$\left.\begin{aligned} \lambda_1 + \lambda_2 + \lambda_3 = (s_{11} + s_{22} - 3) < 0 \\ \lambda_1 \lambda_2 \lambda_3 = (s_{11} + s_{22} - s_{31} - s_{11} s_{22} + s_{12} s_{21} + s_{22} s_{31} - 1) < 0 \end{aligned}\right\} \text{ for } D_1, D_2\,. \tag{23}$$

Jacobian matrix equation, $J_{1,2}$, given in Eq. (22) lets us derive the eigenvalues as $\lambda_1 = -0.4414$, $\lambda_{2,3} = -0.1293 \pm 1.2527i$ based on the equilibrium point $(-0.0857, 0.2857, -0.0857) \in D_{1,2}$. When we consider the same initial conditions for Eq. (21), its outcome will have three roots, which are one negative and two complex conjugates lying in the subspaces with negative real parts, respectively. These roots imply that SC-CNN system is stable and its equilibrium points, $P_{1,2}$, lying on to focus node. When $x_1(t)$ is the variable for the multi-scroll attractor, the $x_1 - x_2$ phase

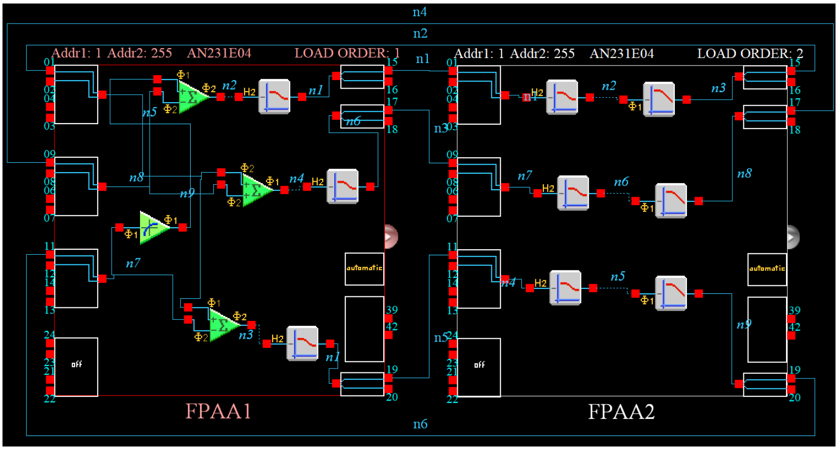

(a)

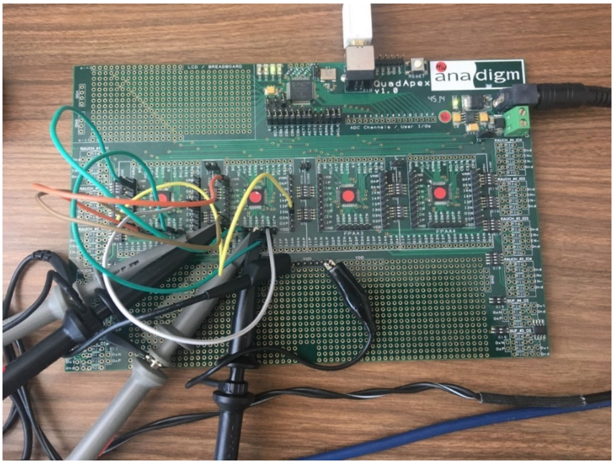

(b)

Fig. 11. Numerical and implementation results of case i: (a) FPAA implementation circuit of Anadigm Designer2 and (b) FPAA hardware implementation.

space becomes as shown in Fig. 12(a). In this part of the proposed study, switching parameter in addition to x_1 state variable has been realized with an error function. Hence, the multi-scroll attractors have been obtained by completing the switched SC-CNN design of the system. In addition, hyperchaos behavior exhibition has been provided with the use of fractional-order design.

The block scheme for the FPAA implementation circuit of AnadigmDesigner 2 is depicted in Fig. 11(a). The analog-based FPAA implementation of the proposed system is realized, as shown in Fig. 11(b). For the numerical simulations, the parameters given in Remark 4 are used. Numerical simulation settings are to generate phase-space data, fixed-step Runge–Kutta integrator in MATLAB 2019 with ODE4 solver is preferred. The simulation time is set to 2500 s, in which time-step is adjusted to 0.1 s.

Figure 12 demonstrates the outcome of multi-scroll attractors with hyperchaotic behavior using fractional-order systems through simulation and implementation results for case I. The phase-space exhibition of multi-scroll in $x_1 - x_2$ plane is shown in Fig. 12(a), while its $x_2 - x_3$ plane representation is given in Fig. 12(b). Among the time series of state variables, x_1(t) state variable is selected to illustrate in Fig. 12(c) due to the reason y_3 output function is used for switching in x_1. The phase-space

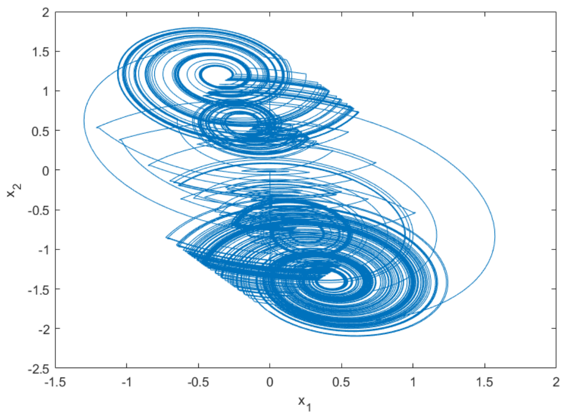

(a)

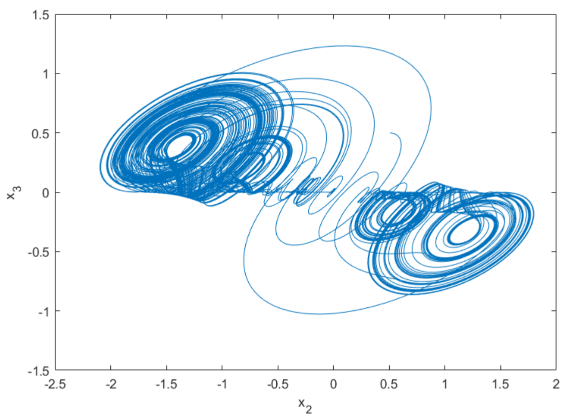

(b)

Fig. 12. Numerical and implementation results of case i: (a) multi-scroll in x_1–x_2 plane, (b) multi-scroll in x_2–x_3 plane, (c) time series of $x_1(t)$ dynamic for multi-scroll and (d) FPAA implementation result in $x_1(t)$–$x_2(t)$ plane.

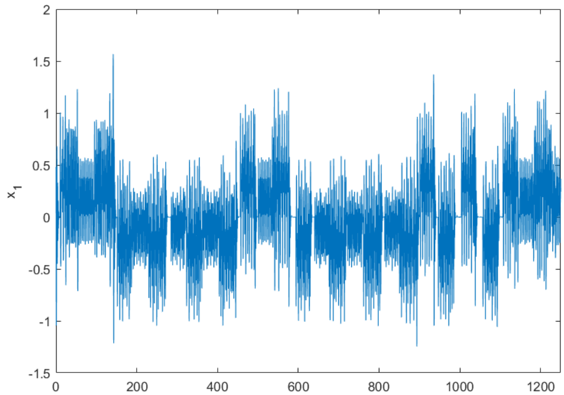

(c)

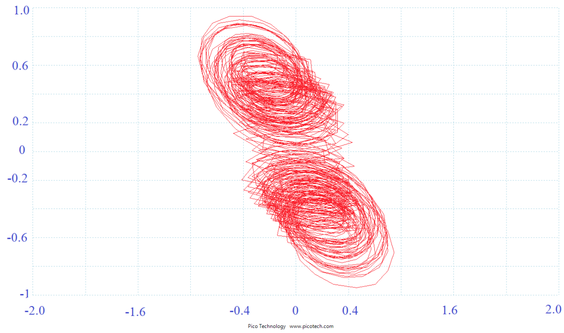

(d)

Fig. 12. (*Continued*)

exhibition of multi-scroll in $x_1 - x_2$ plane for case I is also validated through FPAA implementation in Fig. 12(d).

B. Using 2-Error Function in Fractional-Order Switched SC-CNN-Based Sprott Case H system

Case II: y_3 output function is used for switching in x_1 state variable, while y_2 output function is used for switching in x_3 state variable to obtain multi-scroll attractor.

$$\begin{aligned} D_t^{q1}x_1\pm &= -x_1 + s_{11}x_1 + s_{12}x_2 + [-\mathrm{erf}(ky_3) \pm i_3]\,, \\ D_t^{q2}x_2 &= -x_2 + s_{21}x_1 + s_{22}x_2\,, \\ D_t^{q3}x_3\pm &= -x_3 + s_{31}x_1 + [-\mathrm{erf}(ky_2) \pm i_2]\,, \\ &\left.\begin{aligned} D_t^{q1}x_1+ &= -x_1 + s_{11}x_1 + s_{12}x_2 + [-\mathrm{erf}(ky_3) + i_3] \\ D_t^{q3}x_3+ &= -x_3 + s_{31}x_1 + s_{33}x_3 + [-\mathrm{erf}(ky_2) + i_2] \end{aligned}\right\} \quad \text{switch} \ > 0\,, \end{aligned}$$

$$\left.\begin{array}{l} D_t^{q1}x_1- = -x_1 + s_{11}x_1 + s_{12}x_2 + [-\mathrm{erf}(ky_3) + i_3] \\ D_t^{q3}x_3- = -x_3 + s_{31}x_1 + s_{33}x_3 + [-\mathrm{erf}(ky_2) + i_2] \end{array}\right\} \quad \text{switch} \ < 0\,,$$
$$\begin{array}{l} s_{11} = s_{21} = s_{31} = 1; \quad s_{12} = -1; \quad s_{22} = 1.15; \quad i_2 = 0.5; \quad i_3 = 0.3; \quad k = 100\,, \\ s_{13} = s_{23} = s_{32} = s_{33} = 0, \quad i_1 = 0\,, \\ a_{11} = a_{12} = a_{13} = a_{21} = a_{22} = a_{23} = a_{31} = a_{32} = a_{33} = 0\,. \end{array} \tag{24}$$

In Eq. (24), the equilibrium points lie in two subspaces described in the following. Let D_3 define the subspace, in which x_2 and x_3 are positive, and D_4 define the subspace, in which x_2 and x_3 are negative:

$$\begin{array}{l} D_3 = \{(x_1, x_2, x_3)|x_2, x_3 \geq 0\} : P_3 = (-a_4, -a_5, -a_6)\,, \\ D_4 = \{(x_1, x_2, x_3)|x_2, x_3 < 0\} : P_4 = (a_4, a_5, a_6)\,. \end{array} \tag{25}$$

$$a_4 = \frac{-(i_3 - i_2k - i_3s_{22} + i_2ks_{22})}{(s_{11} + s_{22} - ks_{31} - s_{11}s_{22} + s_{12}s_{21} + k^2s_{21} + ks_{22}s_{31} - 1)}\,,$$

$$a_5 = \frac{-[s_{21}(i_3 - i_2k)]}{(s_{11} + s_{22} - ks_{31} - s_{11}s_{22} + s_{12}s_{21} + k^2s_{21} + ks_{22}s_{31} - 1)}\,,$$

$$a_6 = \frac{(i_2s_{11} - i_2 + i_2s_{22} + i_3ks_{21} - i_3s_{31} - i_2s_{11}s_{22} + i_2s_{12}s_{21} + i_3s_{22}s_{31})}{(s_{11} + s_{22} - ks_{31} - s_{11}s_{22} + s_{12}s_{21} + k^2s_{21} + ks_{22}s_{31} - 1)}\,.$$

In the regions D_3 and D_4, Eq. (24) is linear where its equilibrium points, P^3 and P^4, are derived using the system's *Jacobian matrices*:

$$J_{3,4} = \begin{vmatrix} (s_{11} - 1), & s_{12}, & -k \\ s_{21}, & (s_{22} - 1), & 0 \\ s_{31}, & -k, & -1 \end{vmatrix}\,. \tag{26}$$

The characteristic equation of the system is given by

$$\begin{aligned} S_2(\lambda) = \lambda^3 &+ (3 - s_{11} - s_{22})\lambda^2 + (3 + s_{31} - 2s_{22} - 2s_{11} + s_{11}s_{22} - s_{12}s_{21})\lambda \\ &- s_{11} - s_{21} - s_{22} + s_{31} + s_{11}s_{22} - s_{12}s_{21} - s_{22}s_{31} + 1\,, \end{aligned}$$

where the parameter values are as follows:

$$\begin{array}{l} s_{11} = s_{21} = s_{31} = 1; \quad s_{12} = -1; \quad s_{22} = 1.15; \quad i_2 = 0.5; \quad i_3 = 0.3; \quad k = 100\,; \\ s_{13} = s_{23} = s_{32} = s_{33} = i_1 = 0\,; \\ a_{11} = a_{12} = a_{13} = a_{21} = a_{22} = a_{23} = a_{31} = a_{32} = a_{33} = 0\,. \end{array}$$

Remark 5. System presented in Eq. (24) can generate multi-scroll chaotic attractors by utilizing the circumstances given as follows:

- Adding erf function in x_1 via y_3 nonlinearity;
- Adding erf function in x_3 via y_2 nonlinearity;

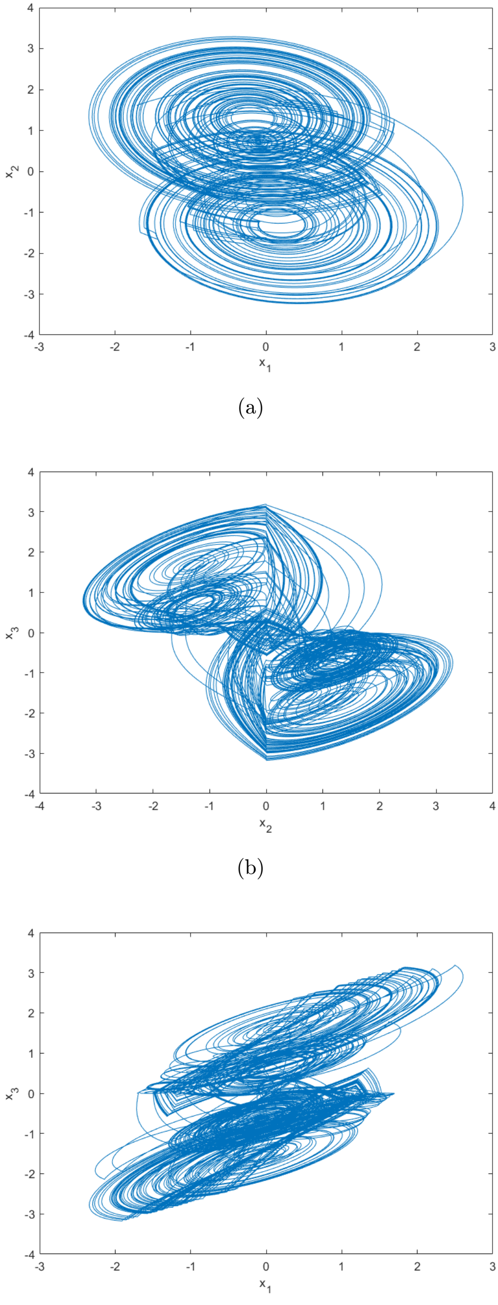

Fig. 13. Numerical and implementation results of case ii: (a) multi-scroll in x_1–x_2 plane; (b) multi-scroll in x_2–x_3 plane; (c) multi-scroll in x_1–x_3 plane; (d) time series of $x_1(t)$ dynamic for multi-scroll; (e) time series of $x_3(t)$ dynamic for multi-scroll and (f) FPAA implementation result in $x_1(t)$–$x_2(t)$ plane.

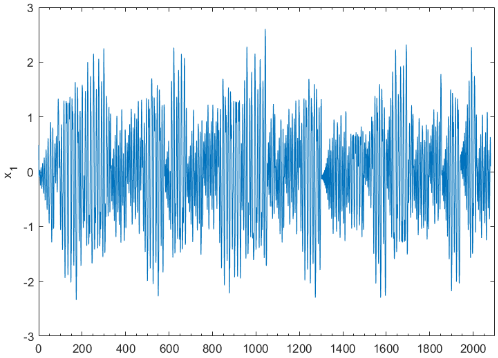

(d)

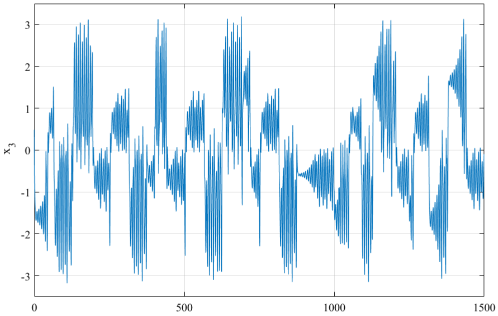

(e)

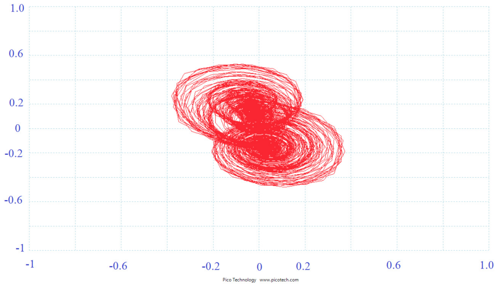

(f)

Fig. 13. (*Continued*)

- Parameters s_{11}, s_{12}, s_{21}, s_{22} and s_{31} satisfy conditions given in Eq. (27).

$$\left.\begin{aligned} \lambda_1+\lambda_2+\lambda_3 &= (s_{11}+s_{22}-3)<0 \\ \lambda_1\lambda_2\lambda_3 &= (s_{11}-s_{12}+s_{22}-s_{11}s_{22}+s_{12}s_{21}-s_{12}s_{31}-1)<0 \end{aligned}\right\} \quad \text{for } D_3, D_4\,. \tag{27}$$

Jacobian matrix equation, $J_{3,4}$, given in Eq. (26) lets us derive the eigenvalues as $\lambda_1 = 0.0780$, $\lambda_{2,3} = -0.4640 \pm 1.3066i$ based on the equilibrium point $(-0.2, 1.33, -1.03) \in D_{3,4}$. When we consider the same initial conditions for Eq. (25), its outcome will have three roots, which are one positive and two complex conjugates lying in the subspaces with negative real parts, respectively. These roots imply that SC-CNN system is unstable and its equilibrium points, $P_{3,4}$, lying on to saddle points. When $x_1(t)$ is the variable for the multi-scroll attractor, the x_1–x_2 phase space becomes as shown in Fig. 13. Herein, the switching parameters in addition to x_1 and x_3 state variables have been realized with two error functions. Hence, the multi-scroll attractors have been obtained by completing the switched SC-CNN design of the system. In addition, hyperchaos behavior exhibition has been provided with the use of fractional-order design. The analog-based FPAA implementation of the proposed system is realized. Figure 13 demonstrates the outcome of multi-scroll attractors with hyperchaotic behavior using fractional-order systems through simulation and implementation results. It is observed that the implementation results verify theoretical and simulation outcomes.

In the fourth section of this paper, error function is utilized to increase the number of equilibrium points and to generate multi-scroll structure. In this section, the outcomes of simulations and implementation results obtained using the proposed error function are given in Fig. 12 for case I and Fig. 13 for case II. Herein, it can be observed that the usage of the error function increased the number of scrolls.

Figure 13 demonstrates the outcome of the proposed method for case II, where an increase in the number of scroll is expected. The phase-space exhibitions of multi-scrolls in x_1–x_2, x_2–x_3 and x_1–x_3 planes are shown in Figs. 13(a)–13(c), respectively. Herein, it should be observed that the number of scroll in case II is more than it was in case I, as expected. Among the time series of state variables, $x_1(t)$ and $x_3(t)$ states variable are selected to illustrate in Figs. 13(d) and 13(e), respectively, due to the reasons y_3 and y_2 output functions are used for switching in x_1 and x_3. The phase-space exhibition of multi-scroll in x_1–x_2 plane for case II is also validated through FPAA implementation in Fig. 13(f).

5.1. *Discussion*

Multi-scroll chaotic attractor generation has always been one of the remarkable topics among chaos studies. The main reason behind this is to enhance, improve and increase complexity in selected chaotic structures while obstructing its predictability. This increase in complexity and decrease in predictability are essential requirements for providing reliable communication. Due to the reasons listed above, herein a design approach is proposed to generate multi-scroll attractors with hyperchaotic behavior using fractional-order systems, where an error function triggers the switched SC-CNN. Error function for the first time in the literature, which is differentiable and exhibits close behavior to the sgn function, is utilized. In addition to this structure, the complexity of the given system can be enhanced with the help of adding fractional-order design that transforms the existing system to the hyperchaos. Consequently, Sprott system case H becomes a carrier signal that is highly unpredictable which gives rise to safer and reliable communication.

In hardware implementation, multi-scroll attractors with hyperchaotic behavior using fractional-order systems circuit design can be categorized as reprogrammable circuits FPGA (Field Programmable Gate Array), FPAA, chip for one special application (Application Specific Integrated Circuit — ASIC) and discrete circuit element implementation. Because of being flexible and reconfigurable, FPAAs are more popular in the implementation of nonlinear systems by utilizing analog functions with the help of dynamic reconfigurations.[70] The presence of Op Amps into FPAAs for realizing many blocks restricts the design flexibility due to the reasons: corner frequency, gain, clock frequency, slew rate and saturation voltage.[71,72] On the other hand, analog-based, i.e., Op Amp, FPAA structures help better observing the behaviors of dynamic systems rather than digital-based structures.[72] This advantage provides quite important contributions in the application stage, especially for the application of secure communication, image processing and cryptology.[73–75] AN231K04-QUAD4 type FPAA QuadApex design board that is the product of Anadigm is used in this study. Realization of nonlinear functions with discrete circuit elements has always created process issues. In this point of view, programmable platforms like FPAAs are seen as an alternative solution to these kinds of problems. As a future study, the author thinks of performing further analysis for grid scroll generation in Multi-Switched SC-CNN-based systems.

6. Conclusion

In this paper, a design approach to generate multi-scroll attractors with hyperchaotic behavior using fractional-order systems, where switched SC-CNN was triggered with error function, has been investigated. Sprott Systems Case H is reconstructed with fractional-order switched SC-CNN system. In the proposed method, multi-scroll attractors with hyperchaotic behavior were generated using error function series. Theoretical analysis of the proposed system's dynamical behaviors was scrutinized, while numerical investigation was carried out with equilibrium, Lyapunov exponent, bifurcation diagrams and 0/1 test methods. Numerical results were also verified on an FPAA platform.

Acknowledgment

This study was funded by the Sivas Cumhuriyet University Scientific Research Projects (CUBAP) (SMYO-029).

References

1. R. Kharel, Design and implementation of secure chaotic communication systems, Doctoral dissertation, Northumbria University (2011).
2. N. Al Bassam and A. Zayegh, Chaos-based communication systems, *Chaos Theory* (National and University Library in Zagreb, 2018), Chapter 4, pp. 61–77.
3. L. Kocarev, Chaos-based cryptography: A brief overview, *IEEE Circuits Syst. Mag.* **1** (2001) 6–21.
4. G. Alvarez and S. Li, Some basic cryptographic requirements for chaos-based cryptosystems, *Int. J. Bifurc. Chaos* **16** (2006) 2129–2151.
5. C. E. Shannon, Communication theory of secrecy systems, *Bell Syst. Tech. J.* **28** (1949) 656–715.
6. E. Y. Xie, C. Li, S. Yu and J. Lü, On the cryptanalysis of Fridrich's chaotic image encryption scheme, *Signal Process.* **132** (2017) 150–154.
7. C. Wang, C. Fan and Q. Ding, Constructing discrete chaotic systems with positive Lyapunov exponents, *Int. J. Bifurc. Chaos* **28** (2018) 1850084.
8. Q. Lai, Z. Wan, A. Akgul, O. F. Boyraz and M. Z. Yildiz, Design and implementation of a new memristive chaotic system with application in touchless fingerprint encryption, *Chin. J. Phys.* **67** (2020) 615–630.
9. Q. Lai, Z. Wan, L. K. Kengne, P. D. K. Kuate and C. Chen, Two-memristor-based chaotic system with infinite coexisting attractors, *IEEE Trans. Circuits Syst. II Express Briefs* **68** (2020) 2197–2201.
10. Q. Lai, A unified chaotic system with various coexisting attractors, *Int. J. Bifurc. Chaos* **31** (2021) 2150013.
11. Q. Lai, Z. Wan and P. D. K. Kuate, Modelling and circuit realisation of a new no-equilibrium chaotic system with hidden attractor and coexisting attractors, *Electron. Lett.* **56** (2020) 1044–1046.
12. Q. Lai, B. Norouzi and F. Liu, Dynamic analysis, circuit realization, control design and image encryption application of an extended Lü system with coexisting attractors, *Chaos Solitons Fract.* **114** (2018) 230–245.
13. O. E. Rossler, An equation for hyperchaos, *Phys. Lett. A* **71** (1979) 155–157.
14. J. Suykens and J. Vandewalle, Quasilinear approach to nonlinear systems and the design of n-double scroll ($n = 1, 2, 3, 4, \ldots$), *IEE Proc. Circuits Dev. Syst.* **138** (1991) 595–603.
15. J. Suykens and J. Vandewalle, Generation of n-double scrolls ($n = 1, 2, 3, 4, \ldots$), *IEEE Trans. Circuits Syst. I Fundam. Theory Appl.* **40** (1993) 861–867.
16. J. Suykens and J. Vandewalle, Between n-double sinks and n-double scrolls. *Proc. Int. Symp. Nonlinear Theory and Its Applications* (Katholieke Universiteit Leuven, Belgium, 1993).
17. J. Lü and G. Chen, Generating multiscroll chaotic attractors: theories, methods and applications, *Int. J. Bifurc. Chaos* **16** (2006) 775–858.
18. K. S. Wallace *et al.*, Generation of n-scroll attractors via sine function, *IEEE Trans. Circuits Syst. I Fund. Theory Appl.* **48** (2001) 1369–1372.
19. D. Cafagna and G. Grassi, Hyperchaotic coupled Chua circuits: An approach for generating new n × m-scroll attractors, *Int. J. Bifurc. Chaos* **13** (2003) 2537–2550.
20. D. Cafagna and G. Grassi, New 3D-scroll attractors in hyperchaotic Chua's circuits forming a ring, *Int. J. Bifurc. Chaos* **13** (2003) 2889–2903.
21. S. Ozoguz, A. S. Elwakil and K. N. Salama, N-scroll chaos generator using nonlinear transconductor, *Electron. Lett.* **38** (2002) 685–686.

22. N. Salama Khaled, S. Ozoguz and A. S. Elwakil, Generation of n-scroll chaos using nonlinear transconductors, in *Proc. 2003 Int. Symp. Circuits and Systems, 2003, ISCAS'03*, Vol. 3 (IEEE, 2003), pp.176–179.
23. M. E. Yalçin *et al.*, Families of scroll grid attractors, *Int. J. Bifurc. Chaos* **12** (2002) 23–41.
24. L. P. Shilnikov, A case of the existence of a denumerable set of periodic motions, *Dokl. Akad. Nauk* **160**(3) (1965) 558–561.
25. Y. Si-Min, Circuit implementation for generating three-dimensional multi-scroll chaotic attractors via triangular wave series, *Acta Phys. Sin.* **4** (2005) 1500–1509.
26. J. Lü, F. Han, X. Yu and G. Chen, Generating 3-D multi-scroll chaotic attractors: A hysteresis series switching method, *Automatica* **40** (2004) 1677–1687.
27. P. Arena *et al.*, Chua's circuit can be generated by CNN cells, *IEEE Trans. Circuits Syst. I Fundam. Theory Appl.* **42** (1995) 123–125.
28. P. Arena *et al.*, State controlled CNN: A new strategy for generating high complex dynamics, *IEICE Trans. Fundam. Electron. Commun. Comput. Sci.* **79** (1996) 1647–1657.
29. P. Arena *et al.*, Generation of n-double scrolls via cellular neural networks, *Int. J. Circuit Theory Appl.* **24** (1996) 241–252.
30. R. Caponetto, M. Lavorgna and L. Occhipinti, Cellular neural networks in secure transmission applications, in *1996 Fourth IEEE Int. Workshop on Cellular Neural Networks and their Applications Proc. (CNNA-96)* (IEEE, 1996), pp. 411–416.
31. P. Arena *et al.*, SC-CNN based systems to realize a class of autonomous and coupled chaotic circuits, in *1997 IEEE Int. Symp. Circuits and Systems (ISCAS)*, Vol. 1 (IEEE, 1997), pp. 581–584.
32. R. Kiliç, M. Alçi and E. Günay, A SC–CNN-based chaotic masking system with feedback, *Int. J. Bifurc. Chaos* **14** (2004) 245–256.
33. R. Kiliç, M. Açi and E. Günay, Two impulsive synchronization studies using SC-CNN-based circuit and Chua's circuit, *Int. J. Bifurc. Chaos* **14** (2004) 3277–3293.
34. E. Günay, M. Alçi and F. Yildirim, An experimental study on chaotic dynamics of CFOA-based SC-CNN circuit, *Int. J. Bifurc. Chaos* **15** (2005) 2551–2558.
35. E. Günay and M. Alçi, Experimental confirmation of SC-CNN-based chaotic masking system, *Int. J. Bifurc. Chaos* **15** (2005) 4013–4018.
36. E. Günay and M. Alç, n-Double scrolls in SC-CNN circuit via diode-based PWL function, *Int. J. Bifurc. Chaos* **16** (2006) 1023–1033.
37. E. Günay, MLC circuit in the frame of CNN, *Int. J. Bifurc. Chaos* **20** (2010) 3267–3274.
38. E. Günay, A new autonomous chaos generator from state controlled-cellular neural networks, *Int. J. Bifurc. Chaos* **22** (2012) 1250069.
39. J. Suykens and H. Anshan, A family of n-scroll attractors from a generalized Chua's circuit, *Arch. Elektron. Uebertrag.* **51** (1997) 131–137.
40. E. Günay and K. Altun, Switched state controlled-CNN: An alternative approach in generating complex systems with multivariable nonlinearities using CNN, *Int. J. Bifurc. Chaos* **28** (2018) 1830019.
41. E. Günay and K. Altun, Lorenz-like system design using cellular neural networks, *Turk. J. Electr. Eng. Comput. Sci.* **26** (2018) 1812–1819.
42. E. Günay and K. Altun, Multi-scroll chaotic attractors in SC-CNN via hyperbolic tangent function, *Electronics* **7** (2018) 67.
43. F. Yu, Z. Zhang, H. Shen, Y. Huang, S. Cai, J. Jin and S. Du, Design and FPGA implementation of a pseudo-random number generator based on a Hopfield neural network under electromagnetic radiation, *Front. Phys.* **9** (2021) 302.

44. F. Yu, L. Li, B. He, L. Liu, S. Qian, Z. Zhang and Y. Li, Pseudorandom number generator based on a 5D hyperchaotic four-wing memristive system and its FPGA implementation, *Eur. Phys. J. Spec. Top.* **230** (2021) 1763–1772.
45. X. Chen, S. Qian, F. Yu, Z. Zhang, H. Shen, Y. Huang and S. Du, Pseudorandom number generator based on three kinds of four-wing memristive hyperchaotic system and its application in image encryption, *Complexity* (2020).
46. F. Yu, H. Shen, Z. Zhang, Y. Huang, S. Cai and S. Du, A new multi-scroll Chua's circuit with composite hyperbolic tangent-cubic nonlinearity: Complex dynamics, Hardware implementation and Image encryption application, *Integration* **81** (2021) 71–83.
47. I. Petras and D. Bednarova, Fractional-order chaotic systems, in *2009 IEEE Conf. Emerging Technologies Factory Automation* (Mallorca, 2009), pp. 1–8.
48. Y. Luo and Y. Chen, *Fractional Order Motion Controls* (Wiley Online Library, 2012), p. 454.
49. B. Ross, The development of fractional calculus, *Hist. Math.* **4** (1977) 75–89.
50. S. H. M. Kilbas and A. J. J. Trujillo, *Theory and Applications of Fractional Differential Equations* (Elsevier, 2006), p. 540.
51. K. S. Miller and B. Ross, *An Introduction to the Fractional Calculus and Fractional Differential Equations* (Wiley, New York, 1993), p. 363.
52. R. Caponetto, G. Dongola, G. Maione and A. Pisano, Integrated technology fractional order proportional-integral-derivative design, *J. Vib. Control* **20** (2014) 1066–1075.
53. T. T. Hartley and C. F. Lorenzo, Dynamics and control of initialized fractional-order systems, *Nonlinear Dyn.* **29** (2002) 201–233.
54. M. H. Sabzalian, A. Mohammadzadeh, S. Lin and W. Zhang, Robust fuzzy control for fractional-order systems with estimated fraction-order, *Nonlinear Dyn.* **98** (2019) 2375–2385.
55. A. Charef, H. Sun, Y. Tsao and B. Onaral, Fractal system as represented by singularity function, *IEEE Trans. Automat. Contr.* **37** (1992) 1465–1470.
56. A. Loverro, Fractional calculus: History, definitions and applications for the engineer, Rapport technique, *University of Notre Dame: Department of Aerospace and Mechanical Engineering* **1**–**28** (2004).
57. E. Tlelo-Cuautle, A. D. Pano-Azucena, O. Guillén-Fernández and A. Silva-Juárez, *Analog/Digital Implementation of Fractional Order Chaotic Circuits and Applications* (Springer, 2020).
58. C. Muñiz-Montero, L. V. García-Jiménez, L. A. Sánchez-Gaspariano, C. Sánchez-López, V. R. González-Díaz and E. Tlelo-Cuautle, New alternatives for analog implementation of fractional-order integrators, differentiators and PID controllers based on integer-order integrators, *Nonlinear Dyn.* **90** (2017) 241–256.
59. D. Matignon, Stability results for fractional differential equations with applications to control processing, *Comput. Eng. Syst. Appl.* **2** (1996) 963–968.
60. M. F. Danca and N. Kuznetsov, Matlab code for Lyapunov exponents of fractional-order systems, *Int. J. Bifurc. Chaos* **28** (2018) 1850067.
61. F. Yang, J. Mou, J. Liu, C. Ma and H. Yan, Characteristic analysis of the fractional-order hyperchaotic complex system and its image encryption application, *Signal Process.* **169** (2020) 107373.
62. J. Sun, M. Peng, F. Liu and C. Tang, Protecting compressive ghost imaging with hyperchaotic system and DNA encoding, *Complexity* **2020** (2020) 8815315.
63. X. Ye, J. Mou, C. Luo and Z. Wang, Dynamics analysis of Wien-bridge hyperchaotic memristive circuit system, *Nonlinear Dyn.* **92** (2018) 923–933.

64. H. Lin, C. Wang and Y. Tan, Hidden extreme multistability with hyperchaos and transient chaos in a Hopfield neural network affected by electromagnetic radiation, *Nonlinear Dyn.* **99** (2020) 2369–2386.
65. J. C. Sprott, Some simple chaotic flows, *Phys. Rev. E* **50** (1994) R647.
66. G. A. Gottwald and I. Melbourne, A new test for chaos in deterministic systems, *Proc. Roy. Soc. A* **460** (2004) 603–611.
67. R. F. Gans, When is cutting chaotic?. *J. Sound Vib.* **188** (1995) 75–83.
68. T. Altun, High-performance optimization methods for emerging power systems, Doctoral dissertation, Arlington University (2020).
69. H. Yin, D. Yu and B. Xia, Reliability-based topology optimization for structures using fuzzy set model, *Comput. Methods Appl. Mech. Eng.* **333** (2018) 197–217.
70. Anadigm, https://anadigm.com/_doc/UM231004-K001.pdf, accessed:2021-06-08.
71. E. Ortega-Torres, C. Sánchez-López and J. Mendoza-López, Frequency behavior of saturated nonlinear function series based on opamps, *Rev. Mex. de Fis.* **59** (2013) 504–510.
72. S. Li, G. Chen and X. Mou, On the dynamical degradation of digital piecewise linear chaotic maps, *Int. J. Bifurc. Chaos* **15** (2005) 3119–3151.
73. J. Hasler and S. Shah, Security implications for ultra-low power configurable SoC FPAA embedded systems, *J. Low Power Electron. Appl.* **8** (2018) 17.
74. I. Cicek, A. E. Pusane and G. Dundar, A new dual entropy core true random number generator, *Analog Integr. Circuits Signal Process.* **81** (2014) 61–70.
75. D. G. Moreno, A. A. Del Barrio, G. Botella and J. Hasler, A cluster of FPAAs to recognize images using neural networks, *IEEE Trans. Circuits Syst. II Express Briefs* **14** (2021) 1.